Single-Turnover Kinetics of *Saccharomyces cerevisiae* Inorganic Pyrophosphatase†

Pasi Halonen,‡,§ Alexander A. Baykov,|| Adrian Goldman,⊥ Reijo Lahti,*,§ and Barry S. Cooperman*,‡

Department of Chemistry, University of Pennsylvania, Pennsylvania 19104-6323, Department of Biochemistry, University of Turku, FIN-20014 Turku, Finland, A. N. Belozersky Institute of Physico-Chemical Biology, Moscow State University, Moscow 119899, Russia, and Institute of Biotechnology, University of Helsinki, P.O. Box 56, FIN-00014 Helsinki, Finland

Received April 24, 2002; Revised Manuscript Received August 12, 2002

ABSTRACT: Soluble inorganic pyrophosphatase (PPase), which converts inorganic pyrophosphate (PP_i) into usable phosphate, is almost universally present as a central enzyme of phosphorus metabolism and uses divalent metal ion as a necessary cofactor. PPase from *Saccharomyces cerevisiae* (Y−PPase) is the best studied with respect to both structure and mechanism. Here we report the first combined use of stopped flow and quenched flow techniques to study the PPase reaction in both the forward (PP_i hydrolysis) and back (PP_i synthesis) directions. The results of these studies permit direct comparison of different divalent metal-ion effects (Mg^{2+}, Mn^{2+}, Co^{2+}) on microscopic rate constants at pH 7.0. For the Mn−enzyme, on which all of the high-resolution X-ray studies have been conducted, they demonstrate that the rate-determining step changes as a function of pH, from hydrolysis of enzyme-bound PP_i at low pH to release of the more tightly bound P_i at high pH. They also provide evidence for two kinetically important forms of the product complex $EM_4(P_i)_2$, supporting an earlier suggestion based on crystallographic evidence, and allow informed speculation as to the identities of acidic and basic groups essential for optimal PPase catalytic activity.

Soluble inorganic pyrophosphatase (PPase[1]), which converts inorganic pyrophosphate (PP_i) into usable phosphate, is almost universally present as a central enzyme of phosphorus metabolism. PPases can be separated into nonhomologous families I and II (*1*, *2*), with family I being the far better studied of the two (*3*−*5*). Scheme 1 presents a kinetic model for catalysis by PPase from *Saccharomyces cerevisiae* (Y−PPase), the best-studied member of family I, in the presence of Mg^{2+} (*6*, *7*). Family I PPase is unique among metal-activated enzymes in having four Mg^{2+} ions at the active site, of which three are essential and one is modulatory (*7*−*9*). Both the three- and the four-metal ion pathways ($n = 1$ and 2, respectively) are physiologically significant, but the latter dominates at Mg^{2+} concentrations that prevail in the cell cytosol. The two pathways have nearly equal k_{cat} values at pH 6.0, but at higher pH values, k_{cat} for the three-metal ion pathway is 2-fold greater. As recently deduced from fluoride inhibition and oxygen exchange data (*6*, *7*), PPase catalysis appears to involve the formation of two enzyme−PP_i intermediates ($EM_{n+2}PP^*$ and $EM_{n+2}PP$, Scheme 1). In accord with recent crystallographic results, in particular the structure of the F^--inhibited substrate complex, we have postulated that $EM_{n+2}PP^*$ to $EM_{n+2}PP$ conversion involves the generation of a low pK_a water molecule, coordinated to two metal ions and located in a suitable position for nucleophilic attack on PP_i (*4*, *5*, *10*).

Scheme 1: PP_i−P_i Equilibration by PPase[a]

$$EM_2 \overset{k_1}{\underset{k_2}{\leftrightarrow}} EM_{n+2}PP^* \overset{k_A}{\underset{k_B}{\leftrightarrow}} EM_{n+2}PP \overset{k_3}{\underset{k_4}{\leftrightarrow}} EM_{n+2}P_2 \overset{k_5}{\underset{k_6}{\leftrightarrow}} EM_{n+1}P \overset{k_7}{\underset{k_8}{\leftrightarrow}} EM_2$$

[a] E = enzyme, M = metal cofactor, P = P_i, PP = PP_i, $n = 1$ or 2.

For Mg^{2+}-activated Y−PPase, all of the rate constants in Scheme 1 have been evaluated at pH 7 (*6*). In addition, k_3 has been evaluated over the pH range 4.8−9.3 (*7*).

Although Mg^{2+} is the physiological cofactor of family I PPases, several other divalent metal ions, including Mn^{2+}, Zn^{2+} , and Co^{2+}, can support its activity in vitro (*11*). The k_{cat} values estimated with the alternative cofactors are 1 order of magnitude lower than that with Mg^{2+} (*11*, *12*), which is largely due to changes in the product binding and release steps. X-ray crystallographic studies of Y−PPase complexed with phosphate (Figure 1) have identified two P_i-binding sites within the active site: P1 and P2. In P1, the phosphate ligands are Arg78, Tyr192, Lys193, and metal ions M3-M4, whereas in P2, which binds the electrophilic phosphoryl group, they are Lys56, Tyr93, and metal ions M1−M4 (*10*, *13*). The P_i-binding affinity for site P2 in Mn−PPase and Co−PPase is 4−5 orders of magnitude greater than that found for Mg−PPase (*12*, *14*). As a result, while the first P_i released following PP_i hydrolysis is from site P2 of Mg−PPase (*8*), for Mn−PPase and Co−PPase, the first P_i released is from site P1 (*14*).

In the present work, we report the combined use of stopped flow and quenched flow techniques to study the PPase reaction in both directions. Our results (a) permit comparison

† This work was supported by grants from NIH (DK13212), the Finnish Academy of Sciences (35736 and 47513), and the Russian Foundation for Basic Research (00-04-48310 and 00-15-97907).

* To whom correspondence should be addressed. B.S.C: tel 215-898-6330; fax 215-898-2037; e-mail cooprman@pobox.upenn.edu. R.L.: tel 358-2-333-6845; fax 358-2-333-6860; e-mail reijo.lahti@utu.fi.

‡ University of Pennsylvania.

§ University of Turku.

|| Moscow State University.

⊥ University of Helsinki.

[1] Abbreviations: HMBP, hydroxymethylene bisphosphonate; PPase, inorganic pyrophosphatase; P_i, phosphate; PP_i, pyrophosphate; Y-PPase, *Saccharomyces cerevisiae* inorganic pyrophosphatase

10.1021/bi026018z CCC: $22.00
Published on Web 09/11/2002

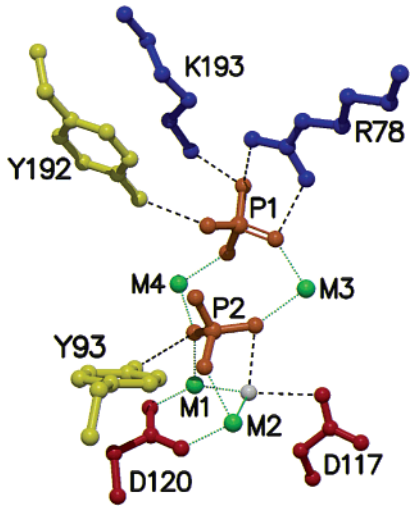

FIGURE 1: Active site of Y−PPase. The Mn_4PPase$(P_i)_2^{up}$ structure (*5*) is displayed.

of the magnitudes of microscopic rate constants measured in the presence of Mg^{2+}, Mn^{2+}, or Co^2, (b) demonstrate that the rate-determining step for the hydrolysis reaction catalyzed by Mn−PPase changes as a function of pH, from hydrolysis of enzyme-bound PP_i at low pH to release of the more tightly bound P_i at high pH, (c) support the existence of two forms of product complex EM_4P_2 in PPase catalysis, and (d) contribute to the elucidation of the catalytic mechanism of Y−PPase.

EXPERIMENTAL PROCEDURES

Materials. The pKW9 plasmid (*15*) containing the yeast wild-type *ppa* gene was transformed into *E. coli* XL2 blue ultracompetent cells. The transformants were grown in 2xYT (*16*) medium and on LA plates (*17*) with 100 μg/mL ampicillin. PPase was expressed and purified as described earlier (*18*), with the omission of the $(NH_4)_2SO_4$ precipitation step due to the separation of Y−PPase from *E. coli* proteins during an earlier DEAE Sepharose chromatography run. After chromatography the sample was over 95% homogeneous, as determined by SDS−PAGE in 12% gels (*19*) and by native PAGE in 7.5−12% gradient gels using Pharmacia PhastSystem. The purified enzyme was concentrated on Amicon Centriprep-10 centrifugal devices, frozen rapidly in liquid N_2, and stored at −70 °C. Enzyme concentrations were calculated on the basis of the subunit molecular mass of 32 kDa (*20*) and $A^{1\%}_{280}$ equal to 14.5 (*8*), or by the Bradford assay (*21*).

Most buffer components (CHES, MES, MOPS, TAPS, TES, and Tris) and EGTA were obtained from Sigma Chemical Co. Acetic acid, sodium acetate, $MgCl_2{\cdot}6H_2O$, $MnCl_2{\cdot}4H_2O$, $CoCl_2{\cdot}6H_2O$, KH_2PO_4 (HPLC grade), and KCl were purchased from Fisher Scientific. Bradford reagent Coomassie Plus was obtained from Pierce. Carrier-free $^{32}P_i$ (as H_3PO_4 in 0.02 M HCl) and carrier-free $^{32}PP_i$ (as $Na_4P_2O_7$ in saline solution) were obtained from NEN-DuPont. $^{32}PP_i$ was removed from $^{32}P_i$ by chromatography on a Dowex-1 column (*22*), after which the purified $^{32}P_i$ contained less than 0.1 mol % $^{32}PP_i$.

Solutions. The following pH buffers were used in the pH ranges indicated: acetic acid-KOH (pH 5.0), MES−KOH (pH 5.5−6.5), MOPS−KOH (pH 7.0), TES−KOH (pH 7.5−8.0), TAPS−KOH (pH 8.5), and CHES−KOH (pH 9.0−10.0). All buffers were used at 0.1 M concentration and adjusted to 0.2 M ionic strength with KCl. All solutions used in the rapid kinetic studies were passed through a filter of pore size 0.45 μm.

Steady-State Measurements. The initial rates of PP_i hydrolysis were estimated from continuous recordings of P_i liberation obtained with an automatic P_i analyzer (*23*). The reaction was initiated by addition of the enzyme. Experiments with Mn^{2+} and Co^{2+} as cofactors were performed at 10 °C at pH ≤8.5, because these cations precipitate as hydroxides at higher pH values. As the PP_i (and P_i) complexes of Mn^{2+} and Co^{2+} easily form aggregates, special care was taken to ensure that the metal ion, PP_i, and P_i concentrations used in these and other experiments were below aggregation levels.

Quenched Flow Measurements. A KinTek model RQF-3 quench flow apparatus with a dead time of ∼5 ms was used. Typically, 15 μL of each of the two solutions, one containing 50−100 μM enzyme and the other containing 10 μM $^{32}PP_i$ (in the forward reaction) or 7 mM $^{32}P_i$ (in the backward reaction) and both containing 2 mM Mn^{2+} or Co^{2+}, were mixed at 10 °C and allowed to react for 3 ms to 20 s before being mixed with 89 μL of the quench solution (0.1 M HCl). The quenched sample was collected in a 1.5 mL plastic vial, to which 45 μL of 4 M CCl_3COOH was added to precipitate the protein. The sample was centrifuged at 13 400*g* for 15 min at 4 °C, and the supernatant was analyzed for $^{32}P_i$ and $^{32}PP_i$, using a molybdate/isobutanol extraction method (*8*). To avoid precipitation of $Mn(OH)_2$ at pH 8.5−10, a pH-jump procedure was used in which the solution of enzyme in the presence of metal ions always contained a diluted (0.02 M) TAPS/KOH buffer, pH 8.0, and the substrate PP_i solution contained a concentrated (0.2 M) buffer of varied pH (pH 8.5−10.0). In this procedure, the metal ions were incubated at high pH for only very short times during the reaction, thus preventing precipitation. Acid denatured enzymes were run and analyzed identically as controls.

Stopped Flow Measurements. An SX.18MV microvolume stopped flow reaction analyzer (Applied Photophysics, Inc.) with a dead time of 2 ms was used. Typically 50 μL samples of each of the two solutions (one containing 5−50 μM enzyme and the other containing an equimolar amount or less of PP_i, both containing 2.0 mM Mn^{2+} or Co^{2+}) were mixed and allowed to react for up to 20 s. In the control runs, PP_i was omitted. Unless otherwise noted, measurements were made under single-turnover conditions ([enzyme] ≥ $[PP_i]$) at 10 °C.

Calculations. Values of k_{SF}, $k_{QF,H}$, and $k_{QF,S}$ (apparent first-order rate constants measured by stopped flow, quenched flow in the direction of PP_i hydrolysis and quenched flow in the direction of PP_i synthesis, respectively) were obtained by fits of the stopped flow and quenched flow data to eq 1 or 2 using SX.18MV instrument control software and Igor Pro 3.16 (Wavemetrics, Oswego, OR). Analysis of biphasic kinetics (substrate binding and hydrolysis) according to the scheme $E + PP_i \rightarrow EPP_i \rightarrow E + 2P_i$ (E = enzyme) was carried out with the global analysis software program Pro-K (Applied Photophysics, Inc.)

$$y = a + Ae^{-kt} \quad (1)$$

$$y = a + A(1 - e^{-kt}) \quad (2)$$

Scheme 2: Simplified Kinetic Model for Mn−PPase

$$(EM_{n+2}PP^{*}+EM_{n+2}PP) \xrightarrow{k_{QF,H}} EM_{n+2}P_2 \xrightarrow{k_5} EM_{n+1}P \xrightarrow{k_7} EM_n$$

Rate constants as a function of pH (Figure 3) were fit to eq 3 using the program SCIENTIST (MicroMath)

$$k = \frac{k_{lim}}{1 + \frac{[H^+]}{K_{ESH2}} + \frac{K_{ESH}}{[H^+]}} \quad (3)$$

where k_{lim} is the pH-independent rate constant, and K_{ESH2} and K_{ESH} are the acid dissociation constants for the essential base and acid, respectively.

Values of k_A, k_B, k_3, k_4, and k_5 for Co−PPase at pH 7.0 were calculated at different fixed values of k_6 by fitting the data shown in Figures 6 and 7 and the measured value of k_{SS} (steady-state first-order rate constant) to equations derived from Scheme 1, using the program SCIENTIST. An iterative procedure was used. First, k_A and k_B were fixed to arbitrary values, and the values of k_3 and k_4 were determined by simultaneously fitting eqs 4 and 5 to the data in Figure 6B. Using these preliminary estimates of k_3 and k_4, values for k_A, k_B and k_5 were further refined by simultaneously fitting eqs 4−6 to the data in Figures 6A and 7. The procedure assumes that $k_{QF,H}$ and k_{SF} describe the disappearance of the quantities $[EM_{n+2}PP^*] + [EM_{n+2}PP]$ and $[EM_{n+2}PP^*] + [EM_{n+2}PP] + [EM_{n+2}P_2]$, respectively (see Results). This fitting cycle was repeated until convergence was obtained

$$d[EM_{n+2}PP^*]/dt = k_B[EM_{n+2}PP] - k_A[EM_{n+2}PP^*] \quad (4)$$

$$d[EM_{n+2}PP]/dt = k_A[EM_{n+2}PP^*] + k_4[EM_{n+2}P_2] - (k_B + k_3)[EM_{n+2}PP] \quad (5)$$

$$d[EM_{n+2}P_2]/dt = k_3[EM_{n+2}PP] + k_6[EM_{n+1}P][P_i] - (k_4 + k_5)[EM_{n+2}P_2] \quad (6)$$

Values of k_5 and k_7 for Mn−PPase at pH 7.0 were found by simulation of Scheme 2, using the program Berkeley Madonna by R. I. Macey & G. F. Oster (http://www.berkeleymadonna.com) and measured values of k_{SF} (70.2 s^{-1}), k_{SS} (5.4 s^{-1}), and $k_{QF,H}$ (89 s^{-1}).

RESULTS

Use of Mn^{2+} and Co^{2+} As Divalent Metal Ion Cofactors. Although Mg^{2+} is the physiological cofactor of Y−PPase, exploratory work with Mg−PPase showed that some of the processes we were interested in proceeded too fast to allow rate constant determination, even at 5 °C, with the rapid quenched flow instrument posing the principal limitation. Accordingly, we turned to the Mn^{2+} enzyme, whose lower catalytic efficiency (*12*) permitted observation of the pH dependence of single-turnover rates of PP_i hydrolysis at 10 °C, as measured either by quenched flow or stopped flow procedures. In addition, the availability of high-resolution X-ray structures of the resting, fluoride-inhibited, and product complex forms of yeast Mn−PPase (*5*, *10*, *13*) permit direct comparison of our results with these earlier structural results.

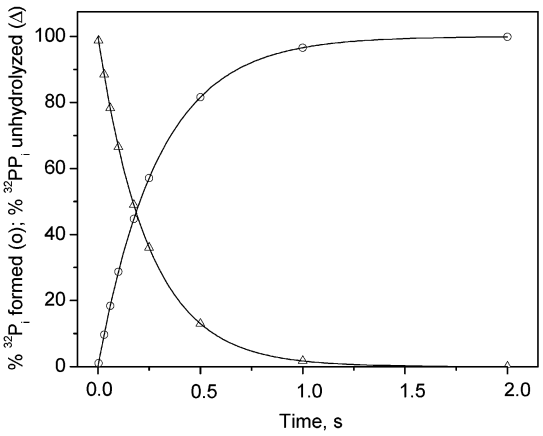

FIGURE 2: Quenched flow analysis: formation of $^{32}P_i$ (○) and disappearance of $^{32}PP_i$ (△). Excess PPase (100 μM, final concentration) was combined with a limiting amount of PP_i (10 μM, final concentration) in pH 5.5 buffer containing 1 mM $MnCl_2$ at 10 °C. Lines represent best fits to eq 1 or 2.

However, Mn^{2+} is unsuitable as divalent metal ion cofactor for studying the back reaction of formation of EPP_i from P_i, since, in its presence the equilibrium constant between EPP_i and $E(P_i)_2$ very strongly favors $E(P_i)_2$ (apparent K_{eq}= 47, *12*). For this purpose we substituted Co^{2+}, which affords considerable EPP_i at equlibrium (apparent K_{eq}= 3.2, *12*). As hydrolytic activity is lower for Co−PPase than for Mn−PPase, the use of Co^{2+} also permitted observation of single-turnover kinetics at 10 °C.

We employed 2.0 mM Mn^{2+} or Co^{2+} in the experiments described below, based on previous results (*12*) showing steady-state PP_i hydrolysis rates to have little dependence on $[Mn^{2+}]$ or $[Co^{2+}]$ in the 1−2 mM range.

pH Dependence of PP_i Hydrolysis by Mn−PPase as Measured by the Quenched Flow Method. Single-turnover experiments were conducted at total [PPase] in large excess (≥10-fold) over both total $[PP_i]$ and K_m such that virtually all PP_i binds rapidly and completely to enzyme prior to rate determining hydrolysis (see below). Results at pH 5.5 are displayed in Figure 2, showing, as expected, indistinguishable rate constants whether measured as PP_i disappearance (4.7 ± 0.4 s^{-1}) or P_i appearance (4.0 ± 0.5 s^{-1}). Values of $k_{QF,H}$ increased with pH (Figure 3), reaching a limiting value of 205 s^{-1} in alkaline media and permitting calculation of an apparent pK_a value of 7.1 for the essential base required in this reaction step (Table 1). The data shown were obtained at an enzyme concentration of 100 μM. Essentially identical results were obtained at a [PPase] of 50 μM, confirming that the value 205 s^{-1} is a true first-order constant.

pH Dependence of PP_i Hydrolysis by Mn−PPase as Measured by the Stopped Flow Method. Metal ion and substrate binding to *Escherichia coli* PPase changes the environment of the active site Tyr55, leading to a large change in its UV spectrum and the appearance of a peak at 243 nm (*24*). In the presence of P_i or the PP_i analogue, hydroxymethylene bisphosphonate (HMBP), the change at 243 nm is seen at (a) lower $[Mn^{2+}]$ than that in their absence and (b) much lower [HMBP] than $[P_i]$, reflecting the higher affinity of *E. coli* PPase for MnHMBP than for MnP_i (*25*). We have observed similar although smaller effects of metal-ion and phosphoryl ligand addition on the A_{243} of yeast PPase (results not shown). Such changes are likely due to perturba-

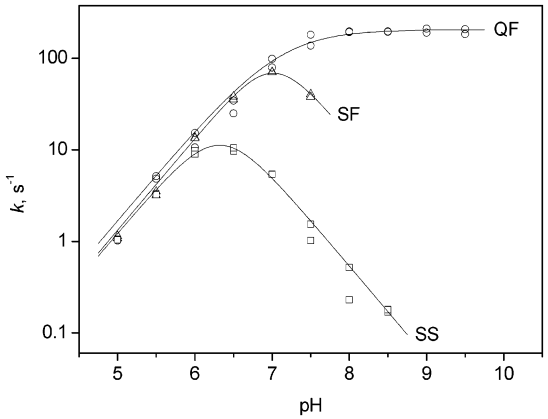

FIGURE 3: pH dependence of the first-order rate constants for Mn−PPase-catalyzed PP_i hydrolysis as estimated from quenched flow (○, QF), stopped flow (△, SF), and steady state (□, SS) kinetics. Lines represent best fits to eq 3. Conditions: 100 μM (quenched flow), 50 μM (stopped flow), or 0.4−4 nM (steady state) PPase; 2 mM $MnCl_2$, 10 (quenched flow) or 50 μM (stopped flow and steady state) PP_i; 10 °C.

Table 1: pH Profile Parameters for Mn−PPase and Co−PPase in PP_i Hydrolysis

parameter	metal	k_{lim} (s^{-1})[a]	pK_{ESH2}	pK_{ESH}[a]
k_{SS}	Mn	>30 (146)	>6.4 (7.1)	<6.4 (5.6)
k_{SF}	Mn	>190 (216)	>7 (7.1)	<7 (6.9)
$k_{QF,H}$	Mn	205 ± 5	7.1 ± 0.1	
k_{SF}	Co	31 ± 9	6.5 ± 0.2	6.4 ± 0.2

[a] Values in parentheses are calculated assuming pK_{ESH2} is equal to 7.1 for k_{SS} and k_{SF} for Mn−PPase (see text).

tion of either Tyr93 in site P2 of Y−PPase (Tyr55 in *E. coli* PPase) or Tyr192 in site P1, or both.

These results permit the selection of an initial PP_i concentration high enough to induce Mn^{2+}-perturbation of A_{243}, but low enough that the P_i concentration resulting from Y−PPase-catalyzed hydrolysis is insufficient to generate a significant ΔA_{243}. As a result, A_{243} increases on $MnPP_i$ binding to enzyme and decreases as Mn^{2+} and P_i are released from enzyme following PP_i hydrolysis, thus allowing stopped flow measurement of Mn−PPase-catalyzed PP_i hydrolysis by monitoring A_{243}.

As shown in Figure 4A, addition of a molar excess of PP_i over PPase leads to three phases of reaction. An initial increase in A_{243} (phase 1) is followed by a period of no change (phase 2) and ultimately by a decrease in A_{243} back to its original value (phase 3). At fixed PPase, phase 1 proceeds more rapidly as [PP_i] is increased (Figure 4B) and phase 2 is lengthened, while the rate of phase 3 is unaffected. Accordingly, we interpret phases 1, 2, and 3 as representing $MnPP_i$ binding to PPase [with a calculated second-order rate constant, k_1 in Scheme 1, of 2.0×10^7 $M^{-1}s^{-1}$ (pH 5, 5 °C)], steady-state turnover of PP_i, and release of Mn^{2+} and P_i from enzyme as PP_i is fully depleted, respectively. Furthermore, since the highest concentration of PP_i used in Figure 4 produces sufficient P_i (100 μM) to saturate the higher-affinity P2 site, phase 3, with rate constant k_{SF}, must correspond principally to release of P_i from site P1 and an attendant release of Mn^{2+} (M3 or M4) (see also below).

Although k_1 increased too rapidly at higher pH to be measured over a broad pH range, k_{SF} is readily measurable up until pH 7.5 (Figure 5), after which point the changes in

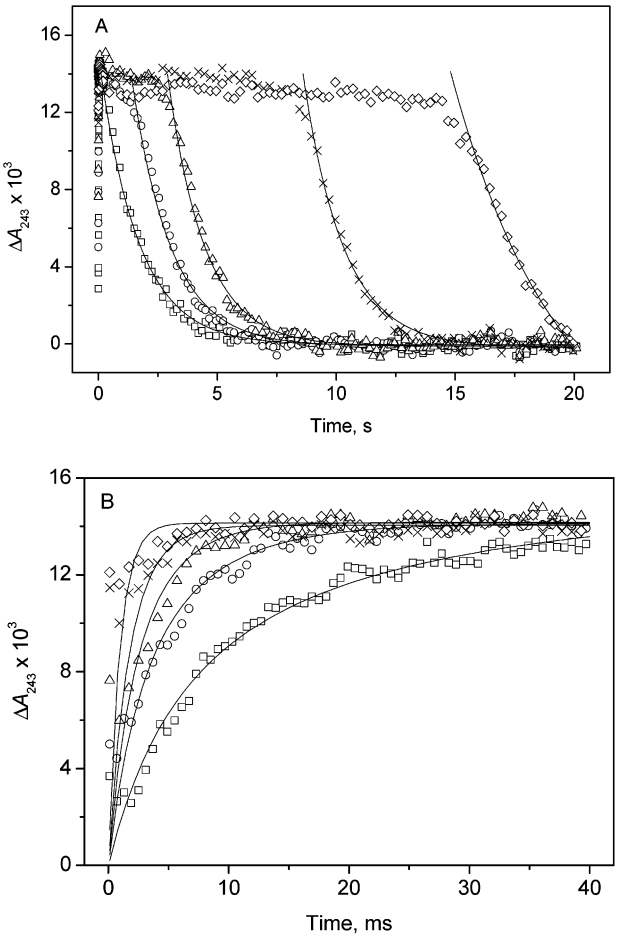

FIGURE 4: Stopped flow analysis: Mn−PPase-catalyzed PP_i hydrolysis monitored at 243 nm (multiple turnovers). PPase (5 μM, final concentration) was combined with different molar excesses of PP_i ($[E]_T$:$[S]_T$ = 1:1 (□), 1:2 (○), 1:3 (△), 1:6 (×), and 1:11 (◇) in buffer, pH 5.0, containing 2 mM $MnCl_2$, at 5 °C). (A) The complete reaction, showing three phases. (B) The initial phase of reaction. Lines represent best fits to eq 1 (panel A, phase 3) or to second-order kinetics (panel B).

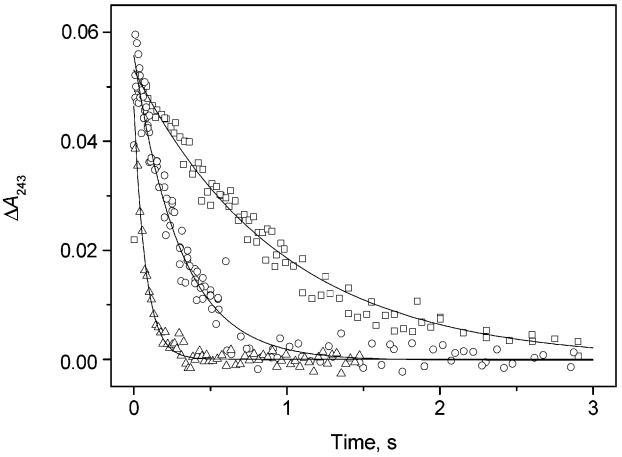

FIGURE 5: Stopped flow analysis: Mn−PPase-catalyzed PP_i hydrolysis monitored at 243 nm (single turnover). PPase (50 μM, final concentration) was combined with a limiting amount of PP_i (50 μM, final concentration) at pH 5.0 (□), 5.5 (○), and 6.0 (△). All samples contained 2 mM $MnCl_2$ at 10 °C. Lines represent best fit to eq 1.

A_{243} are too small to be useful. As is apparent, k_{SF} displays a sharp bell-shaped dependence on pH (Figure 3), reaching

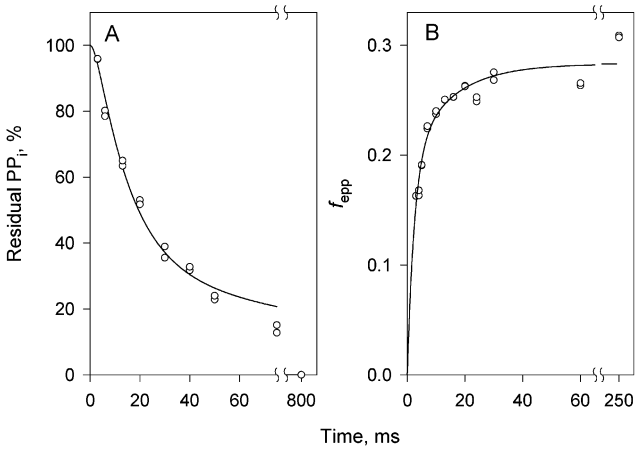

FIGURE 6: Quenched flow analysis: Co−PPase-catalyzed hydrolysis (A) and formation (B) of enzyme-bound PP_i. Lines represent best fits to eqs 4−6. Conditions: 100 μM PPase, pH 7.0, 2 mM $CoCl_2$, 10 μM PP_i (A) or 7 mM P_i (B) (initial concentrations), 10 °C.

its maximum at ∼ pH 7. At pH ≤6.5, k_{SF} is close in value to $k_{QF,H}$, but above this pH the two rate constants diverge, with $k_{QF,H}$ increasing and k_{SF} decreasing. As $k_{QF,H}$ measures the rate of disappearance of $EM_{n+2}PP^*$ and $EM_{n+2}PP$, it follows that k_{SF} must measure the rate of disappearance of $EM_{n+2}PP^*$, $EM_{n+2}PP$, and $EM_{n+2}P_2$. Fitting the pH dependence of k_{SF} to eq 3 requires that $pK_{ESH2} \geq pK_{ESH}$ (Table 1). Accordingly, only a lower limit for the pH-independent value of k_{SF} of >190 s^{-1} could be estimated.

pH Dependence of Mn−PPase Catalyzed Steady-State Hydrolysis of PP_i. Steady-state hydrolysis measurements were conducted at PP_i concentrations in large excess over K_m. In agreement with earlier results (*12*), the pH dependence of k_{cat}, here denoted k_{SS}, follows a sharp bell-shaped curve (Figure 3), with a maximum at ∼ pH 6.1. At pH ≤5.5, k_{SS} is similar in magnitude to both k_{QF} and k_{SF}, but above this pH it falls off rapidly and becomes much smaller than either. On the basis of Scheme 1, we infer that, at pH >6, k_7, the rate constant for $EM_{n+2}P$ disappearance (which has no effect on A_{243}), largely determines k_{SS}.

Co−PPase Catalysis. Quenched Flow Analysis. Single-turnover kinetics for PP_i hydrolysis by Co−PPase at pH 7.0 (Figure 6A) allow determination of $k_{QF,H}$, 30 ± 2 s^{-1}, by application of eq 2. That this value represents a rate constant for PP_i hydrolysis with no significant contribution from the substrate binding step is shown by its essential invariance on 2-fold increases in PPase and/or PP_i concentrations.

Quenched flow measurement at pH 7.0 was also used to determine the rate of enzyme-bound PP_i formation on addition of Co−PPase to 7.0 mM P_i. This concentration of P_i is fully saturating for site P2 and near saturating for P1 (apparent K_d = 3 ± 1 mM, measured at 25 °C, *14*).The quenched flow data presented in Figure 6B indicate that, at equilibrium, f_{epp}, the fraction of enzyme containing bound PP_i, is equal to 0.27 (the equilibrium concentration of PP_i in solution under these conditions is <1 μM and could be neglected), in good agreement with previous results (*14*). Fitting the data in Figure 6B to eq 2 yielded a rate constant, $k_{QF,S}$ = 213 s^{-1}.

Co−PPase Catalysis. Stopped Flow and Steady-State Analyses. Monitoring changes in A_{243} permitted stopped flow analysis of Co−PPase catalysis of PP_i hydrolysis, similar to what was observed for Mn−PPase catalysis. Sample data at pH 7.0 are shown in Figure 7A. As may be seen, substrate binding was slower with Co−PPase than with Mn−PPase, permitting evaluation of k_1 at pH 7.0 (1×10^8 $M^{-1}s^{-1}$). k_{SF} was also smaller for Co−PPase than for Mn−PPase, but its pH dependence was qualitatively similar (Figure 7B), permitting calculation of the pK_a values shown in Table 1.

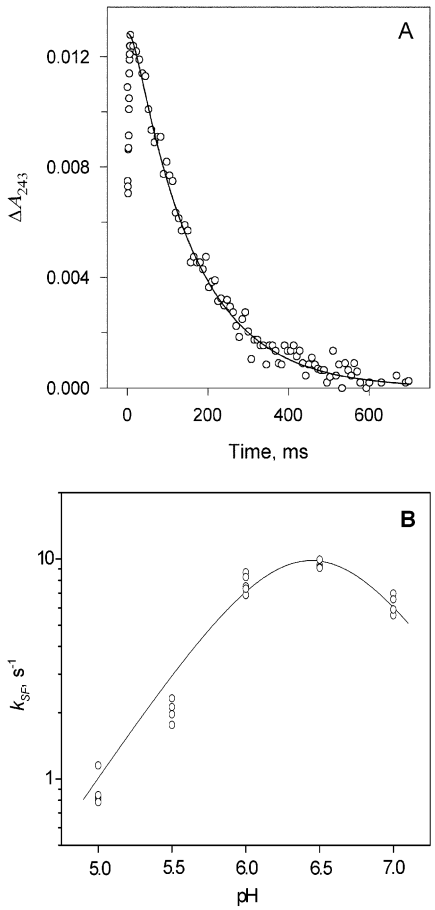

FIGURE 7: Stopped flow analysis of Co−PPase-catalyzed PP_i hydrolysis monitored at 243 nm. (A) PPase (50 μM, final concentration) was combined with a limiting amount of PP_i (50 μM, final concentration) at pH 7.0. All samples contained 2 mM $CoCl_2$ at 10 °C. The solid line represents the best fit to eqs 4−6 (Scheme 1) assuming rapid P_i binding to site P1. (B) pH dependence of the first-order rate constants for Co−PPase-catalyzed PP_i hydrolysis as estimated from stopped flow measurements. Conditions: 5−50 μM PPase; 5−50 μM PP_i; 10 °C; 2.0 mM $CoCl_2$. Line represents best fit to eq 3.

Finally, k_{SS} for Co−PPase at pH 7.0 was determined to be 0.79 s^{-1}.

DISCUSSION

Metal-Ion Effects on Microscopic Rate Constants at pH 7.0. Rate constants for Co−PPase catalysis were estimated (Table 2) by fitting the steady-state k_{cat} and the data in Figures 6 and 7 to Scheme 1 (see *Experimental*), assuming three different values of k_6 (in $M^{-1}s^{-1}$): $\geq 3 \times 10^6$, 7×10^4, or 3×10^4. These values correspond, respectively, to the rate of P_i binding to site P1 (a) not affecting (rapid binding), (b) affecting (partially rate-determining), or (c) fully determining the apparent first-order rate constant of EPP formation at 7 mM P_i (213 s^{-1}). As may be seen, the magnitudes of k_A, k_5, k_7, and k_3/k_4 are largely independent of the value of k_6,

Table 2: Microscopic Rate Constants for Scheme 1 at pH 7.0

parameter	Co−PPase[a]			Mn−PPase[a]	Mg−PPase[b]
k_1 ($M^{-1}s^{-1}$)	$1.0 \pm 0.1 \times 10^8$	$1.0 \pm 0.1 \times 10^8$	$1.0 \pm 0.1 \times 10^8$	$2.0 \pm 0.2 \times 10^{7}$[c]	3.8×10^8
k_A (s^{-1})	68 ± 5	56 ± 4	55 ± 4	> 100	840−2200
k_B (s^{-1})	25 ± 9	29 ± 7	indeterminate		33−34
k_3 (s^{-1})	290 ± 50	1700 ± 1000	indeterminate	> 100	1400
k_4 (s^{-1})	85 ± 7	450 ± 250	indeterminate		350
k_5 (s^{-1})	9.3 ± 0.4	9.4 ± 0.4	9.3 ± 0.4	260[d]	800
k_6 ($M^{-1}s^{-1}$)	$(\geq 3 \times 10^6)$[d]	(7×10^4)[d]	(3×10^4)[d]		
k_7 (s^{-1})	0.87 ± 0.08	0.87 ± 0.08	0.87 ± 0.08	5.7[e]	960−3300

[a] Measured at pH 7.0, 10 °C, 0.2 M ionic strength, 2 mM $MnCl_2$ or $CoCl_2$, except as otherwise indicated. [b] Measured at pH 7.2, 25 °C, 0.1 M ionic strength, 5 mM free Mg^{2+} (*6*). [c] Measured at pH 5.0, 5 °C. [d] Assumed value—see text. [e] Values for k_5 and k_7 were obtained by simulating this reaction according to Scheme 2 taking $k_{QF,H} = 89\ s^{-1}$.

whereas the estimated values of k_3 and k_4 increase markedly as k_6 decreases, becoming indeterminate when P_i binding is rate-determining.

The microscopic rate constants reported in Table 2 permit comparison of divalent metal ion effects on the catalytic efficiency of Y−PPase. Comparing Co−PPase and Mg−PPase, allowing a factor of 2−3 for the 15 °C difference between experiments and assuming that P_i binding to site P1 is not fully rate-determining for EPP formation, leads to the conclusion that the rate constants for the chemical steps of hydrolysis and resynthesis, k_3 and k_4, are similar, at least at pH 7. The major difference concerns the rate constants for P_i release, which are 2−3 orders of magnitude slower for Co^{2+} than for Mg^{2+}. The rate constant for $EM_{n+2}PP^*$ conversion to $EM_{n+2}PP$, k_A, is also significantly lower for Co−PPase than for Mg−PPase. These slower rates correlate with higher affinities of Co−PPase for both PP_i and P_i (*12*, *14*). Thus, whereas the biologically important Mg−PPase has evolved into close to a "perfect" enzyme (*26*) with all four of its forward first-order rate constants k_A, k_3, k_5, and k_7 having similar magnitude, this is not the case for Co−PPase, for which both substrate and products bind with affinities that are too high for optimal turnover.

For Mn−PPase, the PP_i hydrolysis (k_3 step) is practically irreversible, precluding estimation of k_A, k_B, k_3, and k_4, and rate constants were evaluated by fitting to Scheme 2. Nevertheless, it is clear for this enzyme as well that product release is uniquely rate determining, although in this case release of the first P_i is relatively rapid and the slow is the release of the second P_i. This result correlates with the very high affinity previously measured for the 1:1 Mn−PPase:P_i complex (*7*, *12*, *14*).

The pH Dependence of Mn−PPase Catalysis of PP_i Hydrolysis. The three different rate constants measuring Mn−PPase activity each show different pH dependence (Figure 3): $k_{QF,H}$ depends on deprotonation of a single group with apparent pK_a 7.1 (Table 1), whereas both k_{SF} and k_{SS} show pH maxima, the latter of which is shifted to lower pH. It is an attractive hypothesis that the essential basic group modulating $k_{QF,H}$ is the same for all three rate constants. In consequence, the step governed by $k_{QF,H}$ (enzyme-bound PP_i hydrolysis) is rate-determining for all three at low pH, but as the pH is increased and conversion to $EM_{n+2}P_2$ becomes rapid, k_5 becomes rate-determining for k_{SF} and k_7 becomes rate-determining for k_{SS}, with apparent pK_as for the essential acids of 6.9 and 5.6, respectively.

Implications for the Catalytic Mechanism of Y−PPase. The present results provide important support for the catalytic mechanism of Y−PPase recently proposed by us on the basis of high-resolution crystallographic analyses of Mn−PPase (*5*). In the EMn_2 complex, the Mn^{2+} ions bound in positions M1 and M2 are separated by two water molecules, whereas in the inhibited substrate complex EMn_4:F^-:PP, the F^- ion, which mimics the nucleophilic water/hydroxide, is bound directly to both M1 and M2. We speculated that EMn_4PP^* corresponds to a complex in which M1 and M2 are separated by two water molecules, and that deprotonation of one of these waters is required for rapid conversion to the EMn_4PP complex, in which both M1 and M2 bind directly to the nucleophilic hydroxide/water (*4*). This speculation is directly supported by the pH dependence of $k_{QF,H}$ and allows the plausible assignment of the group with the apparent pK_a value of 7.1 to one of the two water molecules bridging M1 and M2 in EMn_4PP^*.

Scheme 3: PP_i−P_i Equilibration by PPase Inferred from Crystallographic Studies[a]

$$EM_2 \underset{k_2}{\overset{k_1}{\leftrightarrow}} EM_{n+2}PP^* \underset{k_B}{\overset{k_A}{\leftrightarrow}} EM_{n+2}PP \underset{k_4}{\overset{k_3}{\leftrightarrow}} EM_{n+2}P_2 \underset{k_D}{\overset{k_C}{\leftrightarrow}} EM_{n+2}P_2^* \underset{k_6}{\overset{k_5}{\leftrightarrow}} EM_{n+1}P \underset{k_8}{\overset{k_7}{\leftrightarrow}} EM_2$$

[a] E = enzyme, M = metal cofactor, P = P_i, PP = PP_i, n = 1 or 2.

In a symmetrical fashion, the earlier proposed catalytic mechanism for Y−PPase (*5*) also includes two forms of the EM_4P_2 complex (Scheme 3), based on direct observation of two crystal forms, one of which has a P2 phosphate oxygen directly bridging M1 and M2, corresponding to the nucleophilic hydroxide in the direction of PP_i hydrolysis, while in the other M1 and M2 are bridged instead by an added water molecule (Figure 1). Consideration of the Co−PPase results provides strong suggestive evidence for such a second form. Thus, our finding that $k_6 \geq 3 \times 10^4\ M^{-1}s^{-1}$ whereas $k_5 = 9.3\ s^{-1}$ (Table 2) leads, according to Scheme 1, to a calculated K_5 ($= k_5/k_6$) value of ≤ 0.3 mM. This is much lower than the measured value of 3 mM (*14*) determined at 25 °C (at 10 °C it is unlikely to be very different). Inclusion of a second EM_4P_2 complex in Scheme 3 obviates this problem, if it is assumed that the apparent k_5 value listed in Table 2 is largely determined by k_C (i.e., $k_5 \gg k_C$) and that both k_6 and k_D are large enough to be consistent with the measured $k_{QF,S}$.

If there are two EM_4P_2 forms, then it is possible that the essential acid modulating k_{SF} (apparent pK_a 6.9) controls the rate of their interconversion. Alternatively, this pK_a could reflect a requirement that MnP_i dissociate from P1 as $MnHPO_4$ rather than $MnPO_4$. Although we have been unable

to find a published value for the pK_a of $MnHPO_4$ in solution, a reasonable estimate is 10 ± 1, and a lower value on the enzyme could be attributed to the high density of positively charged divalent metal ions and amino acid residues (Arg78, Lys56, and Lys193) at the active site (Figure 1). Finally, a likely candidate for the essential acid modulating k_{SS} (pK_a 5.6) is $MnHPO_4$ bound in P2.

Summing up, our results (a) allow comparison of metal ion effects on microscopic rate constants in overall Y−PPase catalysis, (b) demonstrate that the rate-determining step for overall hydrolysis changes from disappearance of enzyme-bound PP_i at low pH to MP_i release at high pH, (c) provide evidence for two kinetically important forms of EM_4P_2, supporting a suggestion based on crystallographic evidence, and (d) allow informed speculation as to the identities of acid and basic groups essential for optimal PPase catalytic activity.

ACKNOWLEDGMENT

We thank Vesa Tuominen for making Figure 1.

REFERENCES

1. Shintani, T., Uchiumi, T., Yonezawa, T., Salminen, A., Baykov, A. A., Lahti, R., and Hachimori, A. (1998) *FEBS Lett. 439*, 263−266.
2. Young, T. W., Kuhn, N. J., Wadeson, A., Ward, S., Burges, D., and Cooke, G. D. (1998) *Micobiology 144*, 2563−2571.
3. Baykov, A. A., Cooperman, B. S., Goldman, A., and Lahti, R. (1999) *Prog. Mol. Subcell. Biochem. 23*, 127−150.
4. Pohjanjoki, P., Fabrichniy, I. P., Kasho, V. N., Cooperman, B. S., Goldman, A., Baykov, A. A., and Lahti, R. (2001) *J. Biol. Chem. 276*, 434−441.
5. Heikinheimo, P., Tuominen, V., Ahonen, A.-K., Teplyakov, A., Cooperman, B. S., Baykov, A. A., Lahti, R., and Goldman, A. (2001) *PNAS 98*, 3121−3126.
6. Baykov, A. A., Fabrichniy, I. P., Pohjanjoki, P., Zyryanov, A. B., and Lahti, R. (2000) *Biochemistry 39*, 11939−11947.
7. Belogurov, G. A., Fabrichniy, I. P., Pohjanjoki, P., Kasho, V., Lehtihuhta, E., Turkina, M. V., Cooperman, B. S., Goldman, A., Baykov, A. A., and Lahti, R. (2000) *Biochemistry 39*, 13931−13938.
8. Springs, B., Welsh, K. M., and Cooperman, B. S. (1981) *Biochemistry 20*, 6384−6391.
9. Baykov, A. A., and Shestakov, A. S. (1992) *Eur. J. Biochem. 206*, 463−470.
10. Heikinheimo, P., Lehtonen, J., Baykov, A., Lahti, R., Cooperman, B. S., and Goldman, A. (1996a) *Structure 4*, 1491−1508.
11. Kunitz, M. (1952) *J. Gen. Physiol. 35*, 423−450.
12. Welsh, K. M., Jacobyansky, A., Springs, B., and Cooperman, B. S. (1983) *Biochemistry 22*, 2243−2248.
13. Harutyunyan, E. H., Kuranova, I. P., Vainshtein, B. K., Höhne, W. E., Lamzin, V. S., Dauter, Z., Teplyakov, A. V., and Wilson, K. S. (1996) *Eur. J. Biochem. 239*, 220−228.
14. Zyryanov, A. B., Pohjanjoki, P., Kasho, V. N., Shestakov, A. S., Goldman, A., Lahti, R., and Baykov, A. A. (2001) *J. Biol. Chem. 276*, 17629−17634.
15. Wood, K. V., Amy Lam, Y., Seliger, H. H., and McElroy, W. D. (1989) *Science 244*, 700−702.
16. Rodriguez, R. L., and Tait, R. C. (1983) *Recombinant DNA Techniques: an Introduction*, p 149, Addison-Wesley, Reading, MA.
17. Sambrook, J., Fritsch, E. F., and Maniatis, T. (1989) *Molecular cloning. A Laboratory Manual*, 2nd ed., Cold Spring Harbor Laboratory Press, Cold, Spring Harbor, NY.
18. Heikinheimo, P., Pohjanjoki, P., Helminen, A., Tasanen, M., Cooperman, B. S., Goldman, A., Baykov, A. A., and Lahti, R. (1996b) *Eur. J. Biochem. 239*, 138−149.
19. Laemmli, U. K. (1970) *Nature 227*, 680−685.
20. Kolakowski, L. F., Jr., Schloesser, M., and Cooperman, B. S. (1988) *Nucleic Acids Res. 16*, 10441−10452.
21. Bradford, M. M. (1976) *Anal. Biochem. 72*, 248−254.
22. Cohn, M. (1958) *J. Biol. Chem. 230*, 3269−3279.
23. Baykov, A. A., and Avaeva, S. M. (1981) *Anal. Biochem. 116*, 1−4.
24. Avaeva, S. M., Rodina, E. V., Kurilova, S. A., Nazarova, T. I., Vorobyeva, N. N., Harutyunyan, E. H., and Oganessyan, V. Yu. (1995) *FEBS Lett. 377*, 44−46.
25. Hyytiä, T., Halonen, P., Salminen, A., Goldman, A., Lahti, R., and Cooperman, B. S. (2001) *Biochemistry* 40, 4645−4653.
26. Knowles, J. R., and Albery, W. J. (1977) *Acc. Chem. Res. 10*, 105−111.

BI026018Z